

# Self-compensation due to point defects in Mg-doped GaN

Giacomo Miceli\* and Alfredo Pasquarello

*Chaire de Simulation à l'Echelle Atomique (CSEA),*

*Ecole Polytechnique Fédérale de Lausanne (EPFL), CH-1015 Lausanne, Switzerland*

(Dated: July, 8 2015)

Using hybrid density functional theory, we address point defects susceptible to cause charge compensation upon Mg doping of GaN. We determine the free-energy of formation of the nitrogen vacancy and of several Mg-related defects. The entropic contribution as a function of temperature is determined within the quasiharmonic approximation. We find that the Mg interstitial shows a noticeably lower free-energy of formation than the Mg substitutional to Ga in *p*-type conditions. Therefore, the Mg impurity is amphoteric behaving like an acceptor when substitutional to Ga and like a double donor when accommodated in an interstitial position. The hybrid-functional results are then linked to experimental observations by solving the charge neutrality equations for semiconductor dominated by impurities. We show that a thermodynamic equilibrium model is unable to account for the experimental hole concentration as a function of Mg doping density, due to nitrogen vacancies and Mg interstitials acting as compensating donors. To explain the experimental result, which includes a drop-off of the hole concentration at high Mg densities, we thus resort to non-equilibrium models. We show that either nitrogen vacancies or Mg interstitials could be at the origin of the self-compensation mechanism. However, only the model based on interstitial Mg donors provides a natural mechanism to account for the sudden appearance of self-compensation. Indeed, the amphoteric nature of the Mg impurity leads to Fermi-level pinning and accounts for the observed drop-off of the hole concentration of GaN samples at high Mg doping. Our work suggests that current limitations in *p*-type doping of GaN could be overcome by extrinsically controlling the Fermi energy during growth.

## I. INTRODUCTION

Gallium nitride is already an essential compound for commercial blue-light-emitting diodes and represents a very promising material for future device applications.<sup>1</sup> Further progress in this field requires achieving high concentrations of free carriers in both *n*-type and *p*-type layers. However, the *p*-type doping efficiency in GaN is still too low and is one of the major problems hampering the widespread use of this material in optoelectronic applications. The Mg impurity substituting Ga, Mg<sub>Ga</sub>, has hitherto been recognized as the only effective acceptor source in GaN.<sup>2,3</sup> Due to its ionization energy of about 220 meV,<sup>4-7</sup> high Mg doping levels are needed in order to achieve significant hole concentrations at room temperature. However, the doping efficiency breaks down at high Mg densities, thereby limiting the hole concentrations that can be achieved in practice.<sup>8-10</sup>

At present, metallorganic vapor phase epitaxy (MOVPE) is the most used technique to grow *p*-type GaN:Mg layers. However, the doping efficiency of as-grown samples is extremely low, due to hydrogen playing a critical passivation role. The hydrogen passivation effect during the growth of GaN:Mg layers has been considered as a beneficial effect. Indeed, the passivation of substitutional Mg impurities keeps the Fermi-level high in the band gap, thereby preventing the formation of compensating donors.<sup>11</sup> The acceptors are then activated through post-growth annealing treatments.<sup>2,12</sup> For samples grown by metallorganic chemical vapor deposition, Kaufmann *et al.*<sup>8</sup> have shown that hydrogen depassivation is very effective in the moderate doping range, i.e. for Mg densities ranging between  $3 \times 10^{18}$  and  $2 \times 10^{19}$  cm<sup>-3</sup>. However, more recently, it has been shown that hydrogen incorporates proportionally with Mg, likely forming

beneficial Mg-H complexes, but saturates at a Mg doping threshold of about  $3 \times 10^{19}$  cm<sup>-3</sup>.<sup>13</sup> Therefore, higher Mg doping densities cannot be achieved through the beneficial passivation effect of hydrogen. In addition, post-growth annealing treatments are not able to entirely remove the hydrogen atoms.<sup>13</sup> As a consequence, part of the Mg<sub>Ga</sub> acceptors are passivated by hydrogen and remain electrically inactive. On the basis of these considerations, the use of hydrogen as a temporary passivating agent during growth does not allow one to envisage higher hole concentrations in GaN.

Molecular beam epitaxy (MBE) has been proposed as an alternative growth technique to overcome the doping limitations described above. In this growth technique, the lower operating temperatures enable higher hole densities, in the absence of any significant hydrogen concentration.<sup>9,10,14</sup> Nevertheless, regardless of the adopted growth technique, all the experimental studies report a drastic drop-off in the hole density upon reaching typical Mg concentrations of about  $10^{19}$  cm<sup>-3</sup>.<sup>8,9,13</sup> Hence, we conclude that the origin of the drop-off should not be related to the occurrence of hydrogen.

The drastic decrease in hole concentration above a Mg doping density of  $10^{19}$  cm<sup>-3</sup> could arise from a deterioration of the sample. Above the solubility limit, the excess of Mg would precipitate forming clusters of new phases causing the degradation of the crystallinity. Such a deterioration in semiconductor samples would dramatically affect the carrier transport properties. However, the measured hole mobility in GaN:Mg does not undergo any dramatic change over the doping range  $3 \times 10^{18}$ – $7 \times 10^{19}$  cm<sup>-3</sup>.<sup>8</sup>

The experimental evidence mentioned above suggests that neither the presence of hydrogen nor the crystalline deterioration can cause the drop-off in the hole concen-

tration at the Mg doping density of about  $10^{19} \text{ cm}^{-3}$ . Hence, a compensation mechanism based on either intrinsic or Mg-related point defects is generally invoked.

In early studies, the key role in the self-compensation process has generally been assigned to the nitrogen vacancy,  $V_N$ .<sup>15–17</sup> Later, the  $\text{Mg}_{\text{Ga}}\text{-}V_N$  defect complex, a deep donor defect in GaN, has been associated with the observed photoluminescence (PL) peak at about 2.9 eV and assumed to be at the origin of the severe compensation in heavily doped GaN:Mg.<sup>8,18</sup> The  $\text{Mg}_{\text{Ga}}\text{-}V_N$  complex has indeed been identified through positron annihilation spectroscopy.<sup>19,20</sup> However, this defect complex turned out to occur only in moderate concentrations ( $\sim 2 \times 10^{17} \text{ cm}^{-3}$ ) and to be unstable against annealing above  $500^\circ\text{C}$ .<sup>19,20</sup> This experimental evidence clearly contrasts with the dominance of the peak at 2.9 eV in the measured PL spectra.<sup>6</sup> The role of the  $\text{Mg}_{\text{Ga}}\text{-}V_N$  complex has further been diminished by a theoretical study,<sup>21</sup> in which the blue luminescence has instead been associated to the substitutional  $\text{Mg}_{\text{Ga}}$  impurity. In a recent theoretical work,<sup>22</sup> the  $V_N$  defect has been found at noticeably lower energies than beforehand,<sup>23</sup> reviving the suggestion that this defect plays a primary role in the compensation. Hence, despite the importance of the technological implications and the numerous efforts devoted to this problem, the microscopic mechanisms behind the self-compensation process in  $p$ -type GaN:Mg have remained elusive to a large extent.

In this work, we address the self-compensation mechanism in GaN by an extensive investigation of the role played by point defects upon Mg doping. Through hybrid density functional calculations, we first obtain the formation energies of a set of relevant point defects, including the nitrogen vacancy ( $V_N$ ), the magnesium substitutional to gallium ( $\text{Mg}_{\text{Ga}}$ ), the magnesium interstitial ( $\text{Mg}_{\text{inter}}$ ), and the  $\text{Mg}_{\text{Ga}}\text{-}V_N$  defect complex. Among the native donor point defects, the nitrogen vacancy is found to be the most stable defect, in agreement with previous theoretical studies.<sup>23,24</sup> Furthermore, we find that the Mg impurity in GaN shows an amphoteric behavior acting like an acceptor in the form of  $\text{Mg}_{\text{Ga}}$  and like a double donor in the form of  $\text{Mg}_{\text{inter}}$ , when going from  $n$ -type to  $p$ -type conditions. Through the equations of semiconductors dominated by impurities, we link our hybrid-functional results with experimental observations. The amphoteric nature of the Mg impurity is identified as the mechanism causing Fermi-level pinning and as origin of the observed drop-off of hole concentrations in GaN samples with increasing Mg doping.

The article is organized as follows. In Sec. II, the relevant point defects are studied within a hybrid-functional framework. In particular, in Sec. II A, we describe the theoretical formulation for determining the energetics of point defects. The defect formation energies and charge transition levels are given in Sec. II B. In Sec. III, we use the charge-neutrality equations of semiconductors dominated by impurities to investigate the hole concentration as a function of Mg doping density. We focus on equilibrium and non-equilibrium models in Secs. III A and III B, respectively. Conclusions are drawn in Sec. IV.

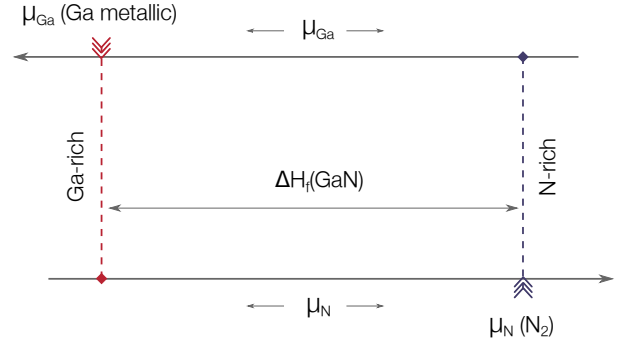


FIG. 1. Schematic representation of the thermodynamically allowed experimental conditions for the growth of GaN. Ga and N chemical potentials can vary within an energy range set by the enthalpy of formation of GaN. The extreme cases are referred to as Ga-rich and N-rich conditions, respectively.

## II. THERMODYNAMICS OF POINT DEFECTS

### A. Formation free energy

In this work, we focus on the defect formation free energy which is a key thermodynamic quantity determining the defect concentration. When a point defect  $X$  is formed in GaN in the charge state  $q$  and at a given temperature  $T$ , the required free energy of formation is defined as follows

$$F^f(X^q; T) = F_{\text{tot}}(X^q; T) - F_{\text{tot}}(\text{GaN}; T) - \sum_{\alpha} n_{\alpha} \mu_{\alpha}(T) + q(\varepsilon_v + \mu_F + \Delta V) + E_{\text{corr}}^q, \quad (1)$$

where  $F_{\text{tot}}(X^q; T)$  and  $F_{\text{tot}}(\text{GaN}; T)$  represent the calculated total free energies for the defective and pristine supercells, respectively.  $n_{\alpha}$  is the number of atoms of the species  $\alpha$  added ( $n_{\alpha} > 0$ ) or removed ( $n_{\alpha} < 0$ ) from the system and  $\mu_{\alpha}(T)$  represents its relative chemical potential.  $\mu_F$  is the electronic chemical potential as referred to the top of the valence band  $\varepsilon_v$ .  $\Delta V$  is an alignment term and  $E_{\text{corr}}^q$  is the correction term due to finite-size effects.<sup>25,26</sup>

The defect formation free energy depends on the relative abundances of the atomic species involved in the growth process, which are set by the choice of the reference elemental chemical potentials. In the case of GaN, the chemical potentials  $\mu_N$  and  $\mu_{\text{Ga}}$  are linked by the equilibrium thermodynamic condition which guarantees the stability of the GaN phase:

$$\mu_{\text{GaN}}(T) = \mu_{\text{Ga}}(T) + \mu_N(T). \quad (2)$$

Depending on the experimental growth conditions,  $\mu_N(T)$  and  $\mu_{\text{Ga}}(T)$  can vary within specific bounds. For Ga and N chemical potentials, the upper bounds are set by the formation of metallic Ga and of the nitrogen molecule, respectively:

$$\mu_{\text{Ga}}(T) \leq \mu_{\text{Ga}}(\text{Ga metallic}; T) \quad (3)$$

$$\mu_N(T) \leq \mu_N(\text{N}_2; T). \quad (4)$$

The following condition holds between the chemical potentials in the extreme cases:

$$\mu_{\text{GaN}}(T) = \mu_{\text{Ga}}(\text{Ga metallic}; T) + \mu_{\text{N}}(\text{N}_2; T) + \Delta H_f(\text{GaN}; T) \quad (5)$$

where  $\Delta H_f(\text{GaN}; T)$  is the formation enthalpy of the GaN compound. Hence, the formation enthalpy of GaN sets the range of variation for the elemental chemical potentials (cf. Fig. 1). In Fig. 1, we schematically represent the range of variation of the elemental chemical potentials which fixes the equilibrium properties of the sample. Any possible thermodynamic condition for growing GaN is represented by a vertical line located between the two thermodynamic extremes corresponding to Ga-rich and N-rich conditions.

As far as magnesium is concerned, we set the chemical potential to a value corresponding to the equilibrium of the compound  $\text{Mg}_3\text{N}_2$ , which is the most stable Mg compound at fixed  $\mu_{\text{N}}$ .<sup>27</sup> Hence, once  $\mu_{\text{N}}$  and  $\mu_{\text{Ga}}$  are set, the Mg chemical potential is obtained from the following equilibrium condition:

$$3\mu_{\text{Mg}}(T) + 2\mu_{\text{N}}(T) = \mu_{\text{Mg}_3\text{N}_2}(T). \quad (6)$$

Vibrational contributions are rarely considered in density-functional studies of defects in solid-state systems,<sup>28–31</sup> as they are generally negligible at room temperature. However, in this work, we need to determine defect concentrations at growth temperatures as high as 1300 K, and finite temperature effects might play an important role. For this reason, we here consider vibrational contributions within the quasiharmonic approximation. In this approximation, the vibrational free energy is expressed in terms of the harmonic frequencies  $\omega_i$  at zero temperature:<sup>32</sup>

$$F_{\text{vib}}(T) = \sum_i \frac{\hbar\omega_i}{2} + \sum_i k_{\text{B}}T \ln \left[ 1 - \exp \left( -\frac{\hbar\omega_i}{k_{\text{B}}T} \right) \right], \quad (7)$$

where the first sum is the zero-point energy and the second sum corresponds to the temperature-dependent entropic contributions. Anharmonic effects are neglected in this approximation. To highlight the corrections going beyond the formation-energy formulation at zero temperature, we rewrite Eq. (1) as

$$F^{\text{f}}(X^q; T) \cong E_{\text{tot}}(X^q) - E_{\text{tot}}(\text{GaN}) - \sum_{\alpha} n_{\alpha} \mu_{\alpha}^0 + q(E_v + \mu_{\text{F}} + \Delta V) + E_{\text{corr}}^q + \Delta E_{\text{QH}}(T), \quad (8)$$

where  $E_{\text{tot}}(X^q)$  and  $E_{\text{tot}}(\text{GaN})$  are the zero-temperature total energies for the defective and pristine supercells, respectively, and  $\mu_{\alpha}^0$  is the zero-temperature chemical potential of the species  $\alpha$ . The zero-point internal energy and the vibrational contributions resulting from the quasiharmonic approximation are included in the term  $\Delta E_{\text{QH}}(T)$ , which is defined as

$$\Delta E_{\text{QH}}(T) = F_{\text{vib}}(X^q; T) - F_{\text{vib}}(\text{GaN}; T) - \sum_{\alpha} n_{\alpha} [\mu_{\alpha}(T) - \mu_{\alpha}^0]. \quad (9)$$

## B. Relevant point defects

The calculations in this work are performed with the hybrid density functional proposed by Heyd, Scuseria, and Ernzerhof (HSE).<sup>33</sup> We include a fraction of Fock exchange equal to 31% to reproduce the experimental band gap of GaN. Structural properties are not significantly influenced by the adopted fraction of Fock exchange.<sup>34</sup> Our computational scheme relies on norm-conserving pseudopotentials and plane-wave basis sets, as made available in the Quantum-ESPRESSO suite of programs.<sup>35</sup> We use the HSE implementation described in Ref. 36. The kinetic energy cutoff for the wave functions is set at 45 Ry. Spin-unrestricted calculations are performed whenever unpaired electrons occur. Defects are modeled starting from a pristine bulk supercell containing 96 atoms and all defect structures are fully relaxed at the hybrid functional level. In the relaxation, the Brillouin zone of the supercell is sampled at the  $\Gamma$  point and the exchange potential is treated as described in Ref. 37.

The energetics and the electronic structure of the optimized defect geometries are then evaluated with a finer  $2 \times 2 \times 2$  Monkhorst-Pack grid in the Brillouin zone of the supercell. We verified the accuracy of this scheme performing calculations with the semilocal density functional proposed by Perdew, Burke, and Ernzerhof (PBE).<sup>38</sup> We focus on the nitrogen vacancy defect for which structural relaxations are most critical. The nitrogen vacancy in its charge state +1 is fully relaxed using both a  $\Gamma$ -point and a  $2 \times 2 \times 2$  mesh of  $\mathbf{k}$  points. The resulting formation energies are found to differ by less than 1 meV.

Throughout this work, we do not explicitly include gallium 3d electrons among the valence states following previous theoretical studies on nitrides.<sup>39</sup> To validate this approximation, we perform PBE calculations with and without 3d states in the valence. The formation energy of the nitrogen vacancy in its charge state +1 is found to be affected by less than 0.1 eV.

The supercell approach to determine the energetics of charged defects requires some specific care due to the occurrence of spurious electrostatic interactions. For an accurate description of the energetics of isolated charged defects we apply state-of-the-art finite-size corrections.<sup>25,26</sup> We note that we will adopt the isolated approximation also for defect densities as high as  $3.5 \times 10^{19} \text{ cm}^{-3}$ . To estimate possible errors, we consider the finite-size energy correction pertaining to these high defect concentrations. In the case of  $q = \pm 1$  charge states, as for  $\text{Mg}_{\text{Ga}}^-$  and  $\text{V}_{\text{N}}^+$ , we obtain an energy correction of 0.075 eV. For  $q = 2$ , as for  $\text{Mg}_{\text{Ga}}^{+2}$ , the correction yields 0.30 eV. In particular, these corrections would affect the charge transition level between the  $\text{Mg}_{\text{Ga}}^-$  and  $\text{Mg}_{\text{Ga}}^{+2}$  states by only 0.075 eV. These errors are sufficiently small to be neglected (cf. discussion in Sec. III B 2).

We investigate the energetics of relevant defects acting as acceptors or donors during the growth process of GaN. As effective acceptor species, we only consider the magnesium impurity substitutional to gallium. Among the

TABLE I. Calculated defect formation energies ( $E_f^q$ ) and charge transition levels ( $\varepsilon_{q/q'}$ ) for relevant charge states ( $q$  and  $q'$ ), compared to previous theoretical work. The Fermi-energy is fixed at the VBM. Energies are in eV. Some of the values taken from Refs. 21–23 are inferred from figures.

Defect		Ga-rich		N-rich		Ref. 22
		Present	Refs. 21 and 23	Present	Refs. 21 and 23	
$\text{Mg}_{\text{Ga}}$	$E_f^0$	2.0	2.0	1.6	–	0.8
	$E_f^{-1}$	2.4	2.3	2.0	–	2.2
	$\varepsilon_{0/-1}$	0.38	0.26	0.38	0.26	1.40
$\text{V}_{\text{N}}$	$E_f^{+3}$	–1.7	–1.0	–0.3	0.3	–3.7
	$E_f^{+1}$	–0.3	–0.1	1.1	1.2	–0.1
	$E_f^0$	3.3	3.2	4.7	4.3	–
	$\varepsilon_{+3/+1}$	0.70	0.47	0.70	0.47	1.83
	$\varepsilon_{+1/0}$	3.63	3.25	3.63	3.25	–
$\text{Mg}_{\text{Ga}}\text{-V}_{\text{N}}$	$E_f^{+2}$	–0.4	0.2	0.5	1.2	–
	$E_f^{+1}$	1.2	2.0	2.1	2.8	–
	$\varepsilon_{+2/0}$	0.80	0.87	0.80	0.87	–
$\text{Mg}_{\text{inter}}$	$E_f^{+2}$	1.1	–	–0.2	–	–

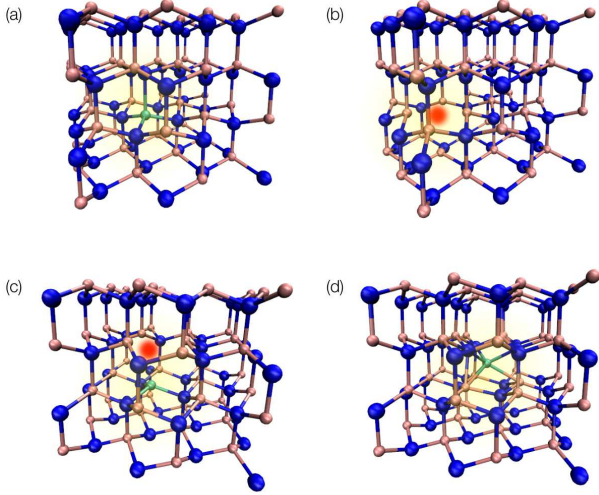


FIG. 2. Atomistic models of various relevant point defects in GaN: (a) the Mg impurity substitutional to Ga ( $\text{Mg}_{\text{Ga}}$ ), (b) the nitrogen vacancy ( $\text{V}_{\text{N}}$ ), (c) the  $\text{Mg}_{\text{Ga}}\text{-V}_{\text{N}}$  complex, and (d) the Mg interstitial. The Mg impurity is shown in green, while the vacancy site is indicated by a blurred red sphere.

possible counteracting donors, we consider  $\text{V}_{\text{N}}$ , the complex  $\text{Mg}_{\text{Ga}}\text{-V}_{\text{N}}$ , and the magnesium interstitial,  $\text{Mg}_{\text{inter}}$ . The relaxed structures of these point defects are illustrated in Fig. 2. The defect formation energies vs. Fermi energy are given Fig. 3.

In its neutral state, the structure of  $\text{Mg}_{\text{Ga}}$  preserves the  $\text{C}_{3v}$  symmetry of wurtzite [cf. Fig. 2(a)]. A hole is well localized on the axial N atom and its trapping is accompanied by a large polaronic lattice distortion, which results in a  $\text{Mg}_{\text{Ga}}\text{-N}$  bond stretched by 15% compared to a regular Ga-N bond. When an electron is added to the defective GaN: $\text{Mg}_{\text{Ga}}$  cell the hole is filled and all the Mg-N bonds become equivalent. The  $\text{Mg}_{\text{Ga}}$  impurity gives rise to a  $0/-1$  acceptor level at 0.38 eV above the valence-band maximum (VBM), in accord with reported experi-

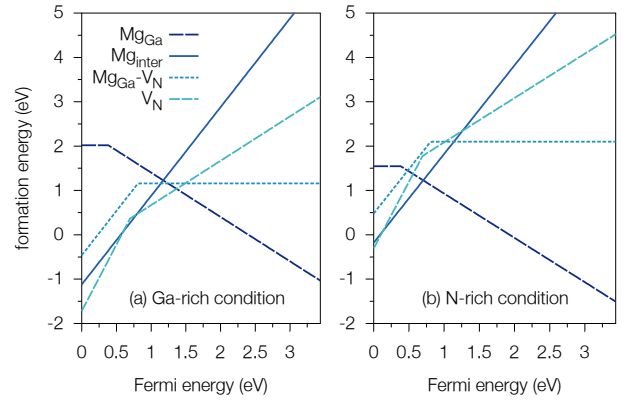


FIG. 3. Calculated formation energies vs. Fermi energy for various relevant point defects in GaN:  $\text{Mg}_{\text{Ga}}$ ,  $\text{Mg}_{\text{inter}}$ ,  $\text{V}_{\text{N}}$ , and the  $\text{Mg}_{\text{Ga}}\text{-V}_{\text{N}}$  complex, in (a) Ga-rich and (b) N-rich conditions.

mental values lying in the range 0.22–0.28 eV.<sup>4–7</sup> We note that the hole localization is well described only when a hybrid density-functional approach is adopted.<sup>21,40,41</sup> The use of semilocal density functionals yields a delocalized electronic state and a defect structure with four Mg-N bonds of similar length.

The nitrogen vacancy ( $\text{V}_{\text{N}}$ ) [cf. Fig. 2(b)] has long been considered the main counteracting donor defect. Indeed, among the native point defects, the nitrogen vacancy is the most stable one for a wide range of Fermi energies within the band-gap.<sup>24,42–44</sup> The nitrogen vacancy is found to be stable in the charge states +1 and +3, with a direct transition at 0.70 eV above the VBM. The neutral and +2 charge states are metastable. In the relaxed structures of the stable charge states, the four nearest-neighbor Ga atoms are displaced away from the vacancy site. This effect becomes larger as the positive charge state of the vacancy increases. The difference between the formation energy of  $\text{V}_{\text{N}}$  in N-rich and Ga-rich conditions corresponds to the formation energy of GaN. Our calculations give 1.4 eV, which favorably compares with



the experimental enthalpy of formation of 1.6 eV.<sup>45</sup>

Another possible counteracting donor is the  $\text{Mg}_{\text{Ga}}\text{-V}_{\text{N}}$  complex [cf. Fig. 2(c)]. The calculated formation energies show that this defect behaves like a double donor in deep  $p$ -type conditions and is neutral otherwise. The corresponding charge transition occurs at 0.80 eV above the VBM. The calculated formation energy implies a moderate defect concentration, in agreement with estimations based on positron annihilation spectroscopy.<sup>19,20</sup> These low densities rule out the  $\text{Mg}_{\text{Ga}}\text{-V}_{\text{N}}$  complex as possible origin of the severe compensation observed in heavily doped samples (cf. Ref. 6).

We summarized in Table II B all the calculated formation energies and charge transition levels. In particular, this table also contains results from previous theoretical studies for comparison.<sup>21–23</sup> In general, our results are in very good agreement with those in Refs. 21 and 23, but differ noticeably from those in Ref. 22. For instance, for  $\text{Mg}_{\text{Ga}}$ , our defect level at 0.38 eV agrees well with the value of 0.26 eV found in Ref. 21, but lies far away from the level of 1.404 eV reported in Ref. 22. Similarly, for  $\text{V}_{\text{N}}$  in N-rich conditions, we find formation energies of 1.1 and  $-0.3$  eV for the  $+1$  and  $+3$  charge states, respectively, in good agreement with the values of  $\sim 1.2$  and  $\sim 0.25$  eV from Ref. 23, but in disaccord with the values of  $\sim -0.15$  and  $\sim -3.7$  eV from Ref. 22. We therefore do not confirm the low formation energies of  $\text{V}_{\text{N}}$  found in the latter work. Furthermore, we remark that the present energies for  $\text{V}_{\text{N}}$  obtained at the hybrid-functional level also agree with those obtained at the semilocal level after proper alignment.<sup>24</sup>

Our investigation also comprises the Mg positioned in an octahedral interstitial site of GaN [Fig. 2(d)]. The interstitial Mg impurity is generally discarded from the outset as an early theoretical study based on semilocal functionals found this defect at higher energies than the substitutional  $\text{Mg}_{\text{Ga}}$ .<sup>27</sup> We find that  $\text{Mg}_{\text{inter}}$  behaves like a double donor irrespective of the position of the Fermi level in the band gap (cf. Fig. 3), and that it becomes noticeably more stable than the substitutional  $\text{Mg}_{\text{Ga}}$  in  $p$ -type conditions. This is consequence of the downwards shift of the VBM achieved with hybrid functionals.<sup>46–48</sup> Our calculations therefore imply a stable interstitial state for the Mg impurity. The Mg impurity in GaN is amphoteric and, depending on the Fermi level, it either behaves like an acceptor in the substitutional site ( $\text{Mg}_{\text{Ga}}$ ) or like a double donor in the interstitial site ( $\text{Mg}_{\text{inter}}$ ). The amphoteric nature of the Mg impurity in GaN could lead to Fermi level pinning.<sup>49,50</sup>

In case the Mg interstitial easily diffuses out of the system, its role as a compensating donor would not apply. This could be particularly critical at the growth temperature of 1300 K. An experimental study has determined the diffusion coefficient of Mg in GaN to follow an Arrhenius behavior, characterized by an activation energy of 1.9 eV and a prefactor of  $D_0 = 2.8 \times 10^{-7} \text{ cm}^2/\text{s}$ .<sup>51</sup> On this basis, we estimate a linear diffusion length of  $0.13 \mu\text{m}$  for a period of two hours, corresponding to typical growth conditions. This distance is short compared to typical layer thicknesses of 1 to  $2 \mu\text{m}$ . Hence, the Mg interstitial is expected to remain trapped within the

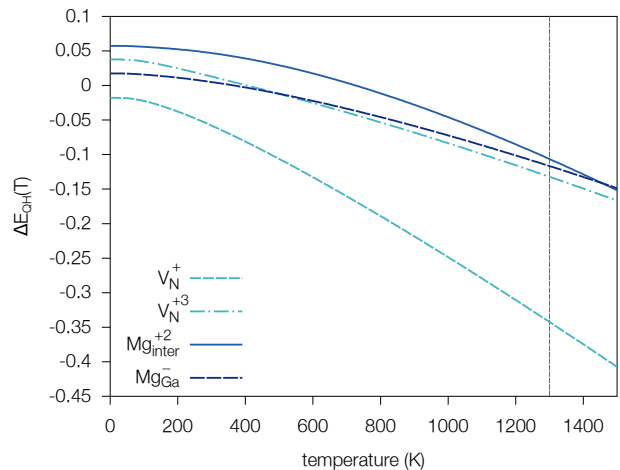


FIG. 4. Calculated correction  $\Delta E_{\text{QH}}(T)$  to the formation-energy formulation at zero temperature for  $\text{V}_{\text{N}}^+$ ,  $\text{V}_{\text{N}}^{+3}$ ,  $\text{Mg}_{\text{inter}}^{+2}$ , and  $\text{Mg}_{\text{Ga}}^{+2}$ . The vertical line indicates the growth temperature of 1300 K.

sample.

To determine the corrections to the formation-energy formulation at zero temperature, we calculate  $\Delta E_{\text{QH}}(T)$  given in Eq. (9) for  $\text{Mg}_{\text{Ga}}$ ,  $\text{Mg}_{\text{inter}}$ , and  $\text{V}_{\text{N}}$  in their stable charge states. For each defect, we evaluate the  $\Gamma$ -point phonons of the supercell using linear-response theory as implemented in Quantum-ESPRESSO.<sup>52</sup> In Fig. 4, the calculated contributions,  $\Delta E_{\text{QH}}(T)$ , as a function of temperature are given. The displayed contribution includes both the zero point motion and the temperature-dependent term [cf. Eqs. (7) and (9)]. As one can notice, at 1300 K, corresponding to the typical growth temperature used in MOVPE, all the defects under investigation undergo an entropic stabilization. For the nitrogen vacancy in its charge state  $+1$ , we observe a significant energy gain of 0.3 eV. For the other defects, the stabilization is smaller and amounts to  $\sim 0.1$  eV.

### III. SELF-COMPENSATION MECHANISMS

The energetics in Fig. 3 suggest that both  $\text{V}_{\text{N}}$  and  $\text{Mg}_{\text{inter}}$  could counteract the  $p$ -doping process. The free energies of formation  $F^f$  given in Eq. (1) cannot directly be compared with experimental data, but determine the defect concentrations at thermodynamic equilibrium. For a given acceptor (A) or donor (D) impurity, the equilibrium concentration is obtained by minimizing the total configurational free energy of the system and reads

$$N_{\text{A/D}} = N_{\text{S}} \exp[-F_{\text{A/D}}^f(\mu_{\text{F}})/k_{\text{B}}T], \quad (10)$$

where  $N_{\text{S}}$  is the number of sites per volume in which the point defect could occur and  $F_{\text{A/D}}^f(\mu_{\text{F}})$  is the free energy of formation which depends on the Fermi energy  $\mu_{\text{F}}$  in the case of charged defects. In the following, we consider self-compensation models which include  $\text{Mg}_{\text{Ga}}$  as an acceptor

and both  $\text{Mg}_{\text{inter}}$  and  $V_N$  as compensating donors. For a given Mg doping density and growth temperature, the respective Boltzmann factors then provide us with the  $V_N$  concentration and the relative abundances of  $\text{Mg}_{\text{Ga}}$  and  $\text{Mg}_{\text{inter}}$ . Since the formation free energies of charged defects depend on the Fermi level, the defect concentrations need to be determined self-consistently along with the Fermi level and the hole concentration  $p$ . Thus, in order to evaluate the compensating role of  $\text{Mg}_{\text{inter}}$  and  $V_N$  upon Mg doping, we resort to the equations of semiconductors dominated by impurities, which allow us to directly link our hybrid-functional results with experimental observations. For a non-degenerate semiconductor at thermodynamic equilibrium, we have:<sup>53</sup>

$$N_A = N_A(\mu_F) \quad ; \quad N_D = N_D(\mu_F) \quad (11)$$

$$p = -\frac{(N_D + \mathcal{K})}{2} + \sqrt{\frac{(N_D + \mathcal{K})^2}{4} + \mathcal{K}(N_A - N_D)} \quad (12)$$

$$\mu_F = E_v - k_B T \ln \left( \frac{p}{\mathcal{N}_v} \right), \quad (13)$$

where  $\mathcal{K} = (\mathcal{N}_v/\beta) e^{-E_A/k_B T}$ ,  $\mathcal{N}_v = 2 (2\pi m_v k_B T/h^2)^{3/2}$  is the effective density of states in the valence band, and  $E_A$  the activation energy of the acceptor state. In these expressions, the valence band degeneracy factor  $\beta = 4$  (Ref. 54) and the valence-band effective mass  $m_v = 0.8$  (Ref. 55) are kept fixed. In view of possible HSE-related inaccuracies,<sup>56</sup> we rigidly shift the calculated band edges to match the activation energy of 0.16 eV used in the analysis of the experimental data of Ref. 8 that we aim at interpreting. Moreover, we neglect any effect resulting from the dependence of  $E_A$  on doping concentration.<sup>9</sup>

In all the presented growth models, we assume Ga-rich conditions which are the experimental thermodynamic conditions at which  $p$ -doped GaN is commonly grown. Within this assumption the nitrogen vacancy concentration is determined self-consistently based on the energetics shown in Fig. 3(a) including free-energy corrections at the given growth temperature, as shown in Fig. 4. Both stable charge states of  $V_N$ , +1 and +3, are taken into account to solve the charge neutrality equations.

In this work the relevant physical quantities are presented as a function of the Mg-doping concentration. Unlike gallium and nitrogen species, the magnesium chemical potential is therefore assumed to vary. The variation of  $\mu_{\text{Mg}}$  does not influence the determination of the relative abundances of  $\text{Mg}_{\text{Ga}}$  and  $\text{Mg}_{\text{inter}}$ . In fact, given a total Mg-doping concentration, the fraction of Mg going into interstitial or substitutional sites can be expressed as the ratio of the respective defect Boltzmann factors, which does not depend on the magnesium chemical potential.

### A. Equilibrium conditions

The solution of Eqs. (11)–(13) gives the acceptor, the donor, and the hole concentrations along with the Fermi energy as a function of the Mg doping concentration at

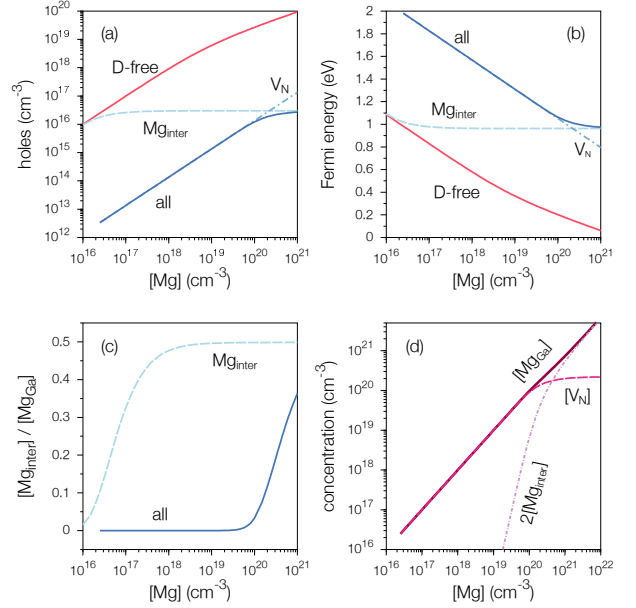


FIG. 5. (a) Hole density and (b) Fermi level as a function of the Mg doping concentration obtained at thermodynamic equilibrium for a growth temperature of 1300 K. The different curves refer to a donor-free model (D-free) and to three compensated models, with  $\text{Mg}_{\text{inter}}$  donors only, with  $V_N$  donors only or with the combined effect of the  $\text{Mg}_{\text{inter}}$  and  $V_N$  donors (all). In panel (c), the ratio  $[\text{Mg}_{\text{inter}}]/[\text{Mg}_{\text{Ga}}]$  is shown as a function of the doping concentration. Panel (d) shows the defect concentrations for the case in which both  $\text{Mg}_{\text{inter}}$  and  $V_N$  act as compensating donors (all).

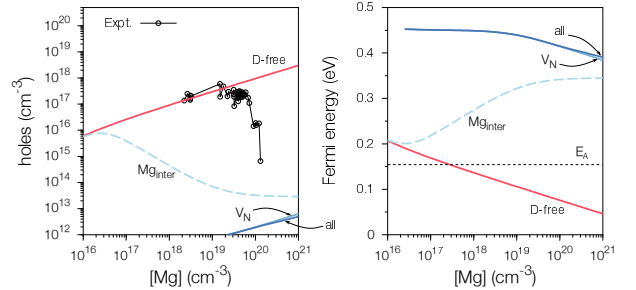


FIG. 6. (a) Hole density and (b) Fermi energy calculated at 300 K while preserving the acceptor and donor concentrations obtained at 1300 K. Experimental data from Ref. 8 are reported in (a) for comparison.

thermodynamic equilibrium. For a typical growth temperature of 1300 K,<sup>8</sup> we obtain the results given in Fig. 5. In particular, in Fig. 5, we distinguish four different compensating models: the ideal case, in which the system is donor-free and all the Mg atoms go into substitutional Ga sites, and three self-compensating models with  $V_N$  donors only, with  $\text{Mg}_{\text{inter}}$  donors only, or with the combined effect of both  $V_N$  and  $\text{Mg}_{\text{inter}}$  donors. In the donor-free case, the absence of donors ensures that the hole concentration reaches its highest value for any Mg doping density and sets an upper limit for more realistic cases. When the formation of both  $V_N$  and  $\text{Mg}_{\text{inter}}$

compensating donors is allowed, the achieved hole densities are radically lower. In particular, we note that for a low Mg doping density the nitrogen vacancies are the dominant counteracting donors. As compared to the donor-free case, their presence keeps the Fermi level at higher values in the band gap for a given Mg doping concentration [Fig. 5 (b)]. However, as soon as the Fermi energy comes closer to the energy level where the formation energies of  $\text{Mg}_{\text{Ga}}$  and  $\text{Mg}_{\text{inter}}$  become equal [the plateau at  $\sim 1$  eV in Fig. 5(b)], i.e. for Mg doping concentrations around  $10^{20} \text{ cm}^{-3}$ , the  $\text{Mg}_{\text{inter}}$  interstitials proliferate giving rise to self-compensation. When only  $\text{Mg}_{\text{inter}}$  are considered as compensating donors, the same proliferation of  $\text{Mg}_{\text{inter}}$  is observed, but at Mg concentrations as small as  $\approx 10^{17} \text{ cm}^{-3}$ . Upon the abrupt proliferation of Mg interstitials, the Fermi level pins and the ratio  $[\text{Mg}_{\text{inter}}]/[\text{Mg}_{\text{Ga}}^-]$  assumes the value of 1/2 [cf. Figs. 5 (b) and (c)]. For a further increase of the Mg doping level, both the hole concentration [Figs. 5(a)] and the Fermi energy [Figs. 5(b)] remain constant and the doping process is abruptly arrested. In this regime, the  $\text{Mg}_{\text{Ga}}$  and  $\text{Mg}_{\text{inter}}$  concentrations increase with a constant ratio 2:1. At variance, the vacancy density remains constant as determined by the pinned Fermi level. We note that in this phenomenology the amphoteric nature of the Mg impurity is critical. Indeed, would  $V_{\text{N}}$  be the only compensating donor, the doping process would have continued, reaching higher hole concentration and lower Fermi levels with increasing Mg doping levels, as shown in Figs. 5(a) and (b), respectively.

In Fig. 5(d), we plot the defect concentrations as a function of the Mg doping density for the model in which both  $V_{\text{N}}$  and  $\text{Mg}_{\text{inter}}$  act as compensating donors. We notice that at low Mg doping densities, the  $V_{\text{N}}$  donor concentration closely follows the increase in  $\text{Mg}_{\text{Ga}}$  concentration, resulting in an immediate compensation. This trend is reflected by the behavior of the Fermi energy, which decreases slowly with increasing Mg doping density [cf. Fig. 5(b)]. At variance, the  $\text{Mg}_{\text{inter}}$  concentration undergoes a sudden increase leading to the abrupt pinning of the Fermi level. The explanation of such a behavior rests on the faster rate of increase of  $[\text{Mg}_{\text{inter}}]$  with respect to  $[V_{\text{N}}]$ . Indeed, while  $[V_{\text{N}}]$  changes as described by Eq. (10),  $[\text{Mg}_{\text{inter}}]$  varies rapidly when the difference in formation energy between  $\text{Mg}_{\text{inter}}$  and  $\text{Mg}_{\text{Ga}}$  becomes comparable to  $k_{\text{B}}T$ . More specifically, through the use of the Boltzmann factors, one obtains

$$[\text{Mg}_{\text{inter}}] = \frac{[\text{Mg}]}{1 + \exp\left(\frac{3(\mu_{\text{F}} - \mu_{\text{F}}^*)}{k_{\text{B}}T}\right)}, \quad (14)$$

where  $\mu_{\text{F}}^*$  is the Fermi level position at which the formation free energies of  $\text{Mg}_{\text{inter}}$  and  $\text{Mg}_{\text{Ga}}$  are equal.

For a direct comparison between theory and experiments, we calculate the equilibrium hole density at room temperature assuming acceptor and donor concentrations as obtained at the growth temperature of 1300 K. This procedure attempts to capture the effects of the rapid thermal quench undergone by the samples, upon which they would preserve the equilibrium defect concentrations achieved at the growth temperature. In Fig. 6,

we give the hole concentrations and the Fermi level at room temperature, as determined through Eqs. (12) and (13) within the various self-compensation models. From Fig. 6(a), one notices that, even for a donor-free case, the hole concentration is much lower than the total  $[\text{Mg}]$  concentration. This effect results from the reduction of the ionized acceptors  $[\text{Mg}_{\text{Ga}}^-]$ , when the decreasing  $\mu_{\text{F}}$  reaches the ionization energy  $E_{\text{A}}$ . Indeed, at a given temperature,  $[\text{Mg}_{\text{Ga}}^-]$  can be expressed as

$$[\text{Mg}_{\text{Ga}}^-] = \frac{[\text{Mg}_{\text{Ga}}]}{1 + \beta \exp\left(-\frac{\mu_{\text{F}} - E_{\text{A}}}{k_{\text{B}}T}\right)}, \quad (15)$$

where  $[\text{Mg}_{\text{Ga}}] = [\text{Mg}_{\text{Ga}}^0] + [\text{Mg}_{\text{Ga}}^-]$  is the total concentration of magnesium substitutional to gallium. The high value of  $E_{\text{A}}$ , as compared to the thermal energy at room temperature, requires heavy doping to achieve high hole concentrations.

For comparison, we also report in Fig. 6(a) the experimental hole densities measured in Ref. 8. In the most realistic case, when both  $\text{Mg}_{\text{inter}}$  and  $V_{\text{N}}$  are acting as compensating donors, the calculated hole density differs from the experimental values by several orders of magnitude. This implies that a model based on the achievement of bulk equilibrium properties does not apply. In fact, the experimental data show that as long as the Mg-doping concentrations remain below a threshold value of about  $10^{19} \text{ cm}^{-3}$ , the achieved hole densities agree with those pertaining to the donor-free model [cf. Fig. 6(a)]. Beyond the threshold concentration of  $\sim 10^{19} \text{ cm}^{-3}$ , the experimental data indicate that the compensation effects intervene severely and suddenly.<sup>8-10,14</sup> The sudden nature of this behavior contrasts with the gradual way in which  $V_{\text{N}}$  compensates the hole concentration at equilibrium conditions [cf. Figs. 5(a) and (d)]. At variance, the amphoteric nature of the Mg impurity and the achievement of Fermi-level pinning through a sudden proliferation of Mg interstitials appear more appropriate to the experimental phenomenology [cf. Fig. 5 (d)].

## B. Non-equilibrium models

In this section, we attempt to identify which donor defect is the dominating compensating defect at the origin of the drop-off in the hole concentration upon Mg doping in GaN, observed at a typical threshold concentration given by  $[\text{Mg}]_{\text{th}} \approx 3.5 \times 10^{19} \text{ cm}^{-3}$  (Ref. 8). We consider either  $\text{Mg}_{\text{inter}}$  or  $V_{\text{N}}$  defects as counteracting donors. More specifically, we assume that Mg incorporates either interstitially or substitutionally:

$$[\text{Mg}] = [\text{Mg}_{\text{inter}}] + [\text{Mg}_{\text{Ga}}]. \quad (16)$$

In our description,  $\text{Mg}_{\text{inter}}$  is always fully ionized, while  $V_{\text{N}}$  only occurs in the charge states +1 for the Fermi energies under consideration (cf. Fig. 3). The charge compensation equation then gives:

$$[\text{Mg}_{\text{Ga}}^-] = 2[\text{Mg}_{\text{inter}}] + [V_{\text{N}}] + p, \quad (17)$$

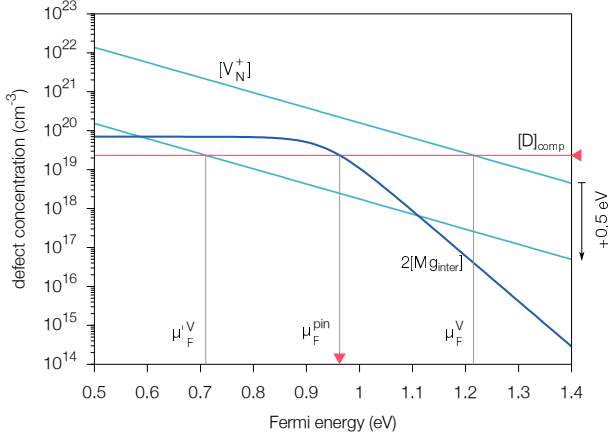


FIG. 7. Concentration of nitrogen vacancy and Mg interstitial as a function of Fermi level.  $[Mg_{inter}]$  is obtained through Eq. (14) at the  $[Mg]_{th}$  doping threshold ( $\approx 3.5 \times 10^{19} \text{ cm}^{-3}$ , from Ref. 8). The factor of 2 accounts for the multiplicity of the  $Mg_{inter}$  donor. We also show the concentration of the nitrogen vacancy when it is destabilized by 0.5 eV. The horizontal line represents the compensating donor concentration  $[D]_{comp}$ .

where  $p$  is the hole density which vanishes at the threshold. Therefore, one can distinguish two different regimes in which either the nitrogen vacancy or the Mg interstitial clearly dominate the counteracting action:

$$2[Mg_{inter}] \ll [V_N] \Rightarrow [Mg_{Ga}^-] = [V_N], \quad (18)$$

$$2[Mg_{inter}] \gg [V_N] \Rightarrow [Mg_{Ga}^-] = 2[Mg_{inter}]. \quad (19)$$

In order to understand the origin of the observed drop-off, we aim at identifying the compensating donor concentration  $D_{comp}$ , beyond which the efficiency of the  $p$  doping process drastically decreases. According to Eqs. (18) and (19),  $D_{comp}$  corresponds to  $[Mg_{Ga}^-]$  at 300 K when the Mg doping density reaches the threshold concentration  $[Mg]_{th}$ , and does not depend on the specific counteracting donor. For convenience, we estimate  $[D]_{comp}$  in case the dominating donor is the Mg interstitial. In this case,  $[D]_{comp}$  is equal to  $2[Mg_{inter}]$  [cf. Eq. (19)] and can be evaluated indifferently at 300 K or at 1300 K, since all interstitial Mg are always fully ionized. At the growth temperature of 1300 K, the defect concentrations are set by equilibrium conditions. The Mg interstitials occur when the Fermi energy reaches the pinning level. Therefore, we assume that the pinning occurs in correspondence of the experimental doping threshold  $[Mg]_{th}$ :

$$\mu_F([Mg]_{th}) = \mu_F^{pin} \quad (20)$$

In correspondence of the pinning, the hole density becomes negligible with respect to the  $2[Mg_{inter}]$  and can thus be neglected in Eq. (17), giving:

$$[Mg_{Ga}^-]_{1300 \text{ K}} = 2[Mg_{inter}] \approx [Mg_{Ga}], \quad (21)$$

where the second approximate equality holds because all the substitutional Mg are ionized at 1300 K, i.e.  $[Mg_{Ga}^0] \approx$

0, since  $\mu_F \gg E_A$  [cf. Eq. (15)]. Combining Eqs. (21) and (16), we then find the following expression for  $[D]_{comp}$ :

$$[D]_{comp} = \frac{2}{3}[Mg]_{th}. \quad (22)$$

The previous analysis is graphically illustrated in Fig. 7. Here, the defect concentrations are plotted as a function of Fermi energy for a temperature of 1300 K. The  $Mg_{inter}$  concentration is calculated through Eq. (14) at the threshold  $[Mg]_{th}$  doping density,<sup>8</sup> while the  $V_N$  concentration is determined through Eq. (10) for Ga-rich conditions. The horizontal line represents the compensating donor concentration  $[D]_{comp}$ . From Fig. 7, we infer that the Fermi level  $\mu_F^V$  at which  $[V_N]$  reaches  $[D]_{comp}$  is larger than the Fermi level  $\mu_F^{pin}$  at which  $[Mg_{inter}]$  reaches  $[D]_{comp}$ . Since the Fermi energy decreases during growth, the condition at  $\mu_F^V$  realizes before that at  $\mu_F^{pin}$ , implying that the nitrogen vacancy is the dominating compensating donor. However, we note that in the hypothetical case in which the nitrogen vacancy is destabilized by 0.5 eV, the situation would be reversed and the  $Mg_{inter}$  would be the principal counteracting donor.

In Sec. III A, we saw that the equilibrium conditions at growth temperature cannot explain the sudden drop-off in the hole density, experimentally observed at  $[Mg]_{th} \approx 3.5 \times 10^{19} \text{ cm}^{-3}$ . The experimental behavior could be reconciled with a Fermi level located at higher energies in the band gap. However, bulk equilibrium conditions would draw the Fermi energy to lower values as the result of self-consistency, leading to more favorable conditions for donor generation and charge compensation. Since the growth takes place at the surface, we abandon the principle that the Fermi level position is determined by sole bulk conditions and assume that it could be affected by specific conditions occurring at the surface. Indeed, due to impurity incorporation, a downwards band-bending has been observed at  $p$ -type GaN surfaces.<sup>57,58</sup> For instance, the measured band bending reaches the value of  $-1.58 \text{ eV}$  for a Mg doping density of  $\sim 5 \times 10^{17} \text{ cm}^{-3}$  (Ref. 57). Such an effect would lead to Fermi levels located at higher energy than those resulting from bulk equilibrium conditions [cf. Fig. 5(b)]. The band bending extends over a surface layer of several hundreds angstroms, in which we propose the defect incorporation takes place. We assume that the formation energies in this region do not differ from their bulk value, neglecting thereby variations that might occur directly at the surface. In the following, we adopt such non-equilibrium models to interpret the experimental evidence.

In the next two subsections, we separately discuss the cases in which the nitrogen vacancy and the  $Mg_{inter}$  are the dominating donors. In particular, we impose that our models reproduce the experimental drop-off in the hole density occurring at  $[Mg]_{th}$ . From such a description, we then infer the dependence of the Fermi level vs. the Mg doping density. We also obtain the defect concentrations of the relevant donors from Eqs. (11).



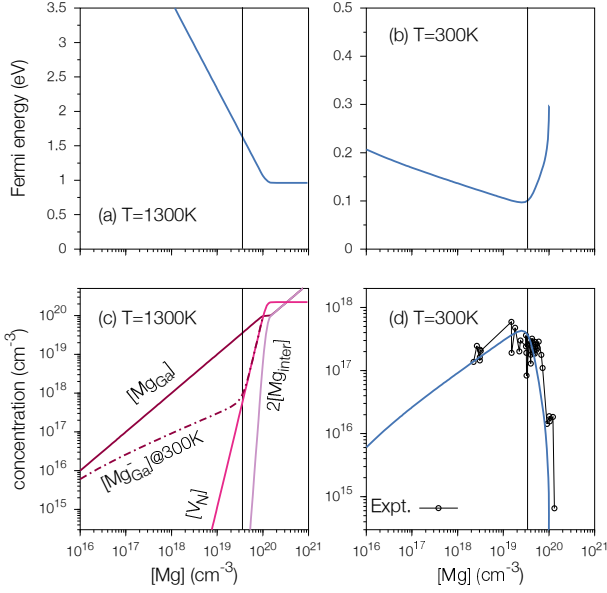


FIG. 8. Non-equilibrium vacancy-dominated self-compensation model designed to interpret the experimental density of holes vs Mg doping concentration [from Ref. 8, panel (d)]: Fermi level (a) at 1300 K and (b) at 300 K, (c) defect concentrations at 1300 K, and (d) hole density at 300 K as a function of Mg doping concentration.

### 1. Nitrogen vacancy as dominating donor

Following the outcome of our calculations (cf. Fig. 7), we first consider a self-compensation model in which the  $V_N$  are the dominating compensating donors. In Fig. 8, we show the evolution of various physical quantities when the model is designed to reproduce the experimental behavior of the hole density vs. Mg doping concentration [cf. Fig. 8(d)]. Figure 8(a) gives the required dependence of the Fermi level during the growth at 1300 K, when the defect structures are formed [cf. Fig. 8(c)]. The hole density at room temperature as adopted in our model is compared with the experimental one in Fig. 8(d).

As shown in Fig. 8(a), the Fermi level at 1300 K monotonically decreases with Mg doping concentration in a similar way as under equilibrium conditions [cf. Fig. 5(b)], but generally remains at higher energies until it reaches the pinning level. In turn, the Fermi energy determines through Eq. (10) the rate at which the compensating  $Mg_{inter}$  and  $V_N$  are formed, as displayed in Fig. 8(c). In Figs. 8(b) and (d), we show the Fermi level and the hole density at 300 K, respectively, while keeping the concentrations of the defect structures achieved at the growth temperature. At 300 K, all  $Mg_{inter}$  and  $V_N$  remain ionized, while the fraction of activated  $Mg_{Ga}$  decreases in a significant way due to the lower temperature [cf. Eq. (15)]. As the Fermi level decreases with Mg doping density, the  $V_N$  concentration increases until it becomes comparable to the  $Mg_{Ga}^-$  concentration, when a drastic decrease of the hole density is observed. In the present model, the nitrogen vacancy is thus the dominating donor defect leading to severe self-compensation.

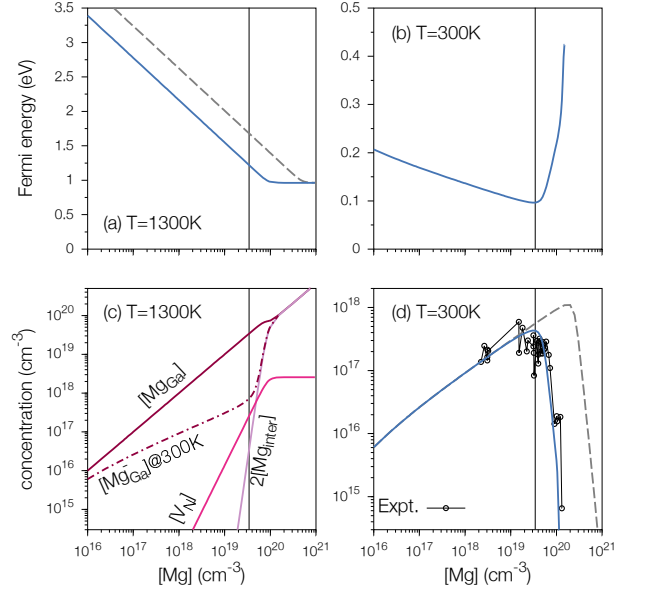


FIG. 9. Non-equilibrium  $Mg_{inter}$ -dominated self-compensation model designed to interpret the experimental density of holes vs Mg doping concentration [from Ref. 8, panel (d)]: Fermi level (a) at 1300 K and (b) at 300 K, (c) defect concentrations at 1300 K, and (d) hole density at 300 K as a function of Mg doping concentration. In panels (a) and (d), the dashed curves indicate a case, in which the drop-off density threshold is shifted to a higher value.

As shown in Fig. 8(c), the proliferation of vacancies strongly counteracts the doping action played by the ionized  $Mg_{Ga}^-$ .

By construction, the present non-equilibrium model reproduces the experimental results [see Fig. 8(d)]. Its validity should therefore be assessed by critically analyzing the behavior of the relevant physical quantities. In particular, we notice that the present model implies a sudden and abrupt proliferation of nitrogen vacancies, in sharp contrast with the behavior observed in equilibrium conditions for  $[V_N]$  (compare Fig. 8 and Fig. 5).

### 2. Magnesium interstitial as dominating donor

In this subsection, we consider a non-equilibrium model in which the dominating donor defects are the  $Mg_{inter}$ . As seen in Fig. 7, our calculations indicate that this can be achieved by destabilizing the vacancy by 0.5 eV. This condition can be realized intentionally in experimental setups through the use of high nitrogen partial pressures during growth.<sup>59–61</sup> This condition could also occur unintentionally in case the thermodynamic conditions do not specifically correspond to the extreme Ga-rich conditions (cf. Figs. 1 and 3). Finally, typical density-functional-theory errors generally amount to a few tenths of electronvolt, but larger errors cannot be ruled out. Therefore, the occurrence of this scenario should be taken under consideration.

From the analysis at the beginning of Sec. III B, we

expect that a destabilization of the vacancy by 0.5 eV should cause the Mg interstitial to become the compensating donor defect, cf. Fig. 7. Following the same procedure as for the case in which the nitrogen vacancy is the dominant compensating donor, we ensure that the model reproduces the drop-off in the hole density as observed experimentally [Fig. 9(d)] and monitor the behavior of the relevant physical quantities, such as the defect concentrations and the Fermi level.

The evolution of the Fermi energy governing the growth process at 1300 K is shown in Fig. 9(a). The Fermi level at 1300 K decreases in a smoother way with respect to the vacancy-dominated model, showing a closer resemblance with the behavior observed under equilibrium conditions [cf. Fig. 5(a)]. The decrease stops when the  $[\text{Mg}_{\text{inter}}]/[\text{Mg}_{\text{Ga}}^-]$  ratio reaches the value of 1/2, corresponding to a sudden proliferation of  $\text{Mg}_{\text{inter}}$ . Upon the pinning of the Fermi level, the concentration of  $\text{V}_{\text{N}}$  reaches a plateau, as can be seen in Fig. 9(c). At the threshold Mg doping density, the hole drop-off is the result of the compensation of the ionized acceptor concentration  $[\text{Mg}_{\text{Ga}}^-]$  at 300 K by the Mg interstitial concentration  $2[\text{Mg}_{\text{inter}}]$  [Fig. 9(c)]. In Figs. 9(b) and (d), we show the associated Fermi level and hole density as found at 300 K.

As remarked for the vacancy-dominated model, the validity of the model should be assessed through the behavior of the relevant physical quantities. Unlike for the vacancy-dominated model, the sudden proliferation of interstitials can be explained in a natural way. Indeed, also in equilibrium conditions, the concentration of interstitials undergoes a sudden increase as a consequence of Fermi level pinning, which occurs when the formation energy of  $\text{Mg}_{\text{inter}}$  and  $\text{Mg}_{\text{Ga}}$  are approximately equal. The abundances of  $\text{Mg}_{\text{inter}}$  and  $\text{Mg}_{\text{Ga}}$  then only depend on their relative energy. At variance, in the vacancy-dominated model, the abundance of nitrogen vacancies in equilibrium conditions depends on the  $\text{V}_{\text{N}}$  formation energy which does not undergo abrupt variations as a function of Fermi level. We also remark that the decay of the Fermi level at 1300 K in the present interstitial-dominated model resembles more closely the behavior observed in equilibrium conditions than in the vacancy-dominated model. In view of these considerations, the abrupt rise of the compensating donor concentration in correspondence of the Mg doping threshold appears more compatible with a response due to Mg interstitials than to nitrogen vacancies.

In the case of a vacancy-dominated self-compensation mechanism, the destabilization of the vacancy might improve the doping efficiency. At variance, in a self-compensation mechanism dominated by Mg interstitials, a change of the thermodynamic conditions would only lead to a small shift of the pinned Fermi level without affecting the overall mechanism.

## IV. CONCLUSIONS

Using a hybrid functional approach, we addressed the energetics of point defects and impurities in GaN that could play an important role in the self-compensation process occurring upon high levels of Mg doping. In particular, our calculations account for the free-energy of formation of the nitrogen vacancy and of several Mg-related defects. Our calculations revealed that the Mg impurity in GaN is amphoteric. It behaves as a single acceptor when substitutional to Ga and as a double donor when it occupies an interstitial site. Our study suggests that only the Mg interstitial and the nitrogen vacancy could act as compensating donors upon Mg doping.

Using the calculated free energies of formation, we then used the equations of semiconductors dominated by impurities to establish a link with experimental observations. These equations were solved self-consistently at thermodynamic equilibrium resulting in the determination of the donor and the acceptor concentrations, the Fermi level position, and the hole density as a function of the Mg doping concentration. Our results indicate that the defect concentrations found under equilibrium conditions are unable to account for the drop-off in the hole density observed experimentally.

We then studied non-equilibrium models which account for the drop-off in the hole density by construction and analyzed the behavior of the relevant physical properties, such as defect concentrations and the Fermi level. In particular, we considered two scenarios in which either the nitrogen vacancies or the magnesium interstitials act as the dominant compensating donors. In both cases, the drop-off in the hole density could only be explained by a sudden proliferation of donor defects. In the case of the vacancy-dominated mechanism, this sudden proliferation contrasts with the behavior found in equilibrium conditions and lacks a physical interpretation. At variance in the case of the interstitial-dominated mechanism, the sudden proliferation is similar to the one observed in equilibrium conditions and stems from the occurrence of Fermi level pinning.

These considerations favor the interpretation in which the dominant compensating donors are Mg interstitials. As long as the Fermi level is high in the band gap, the Mg dopants enter the sample as substitutional impurities. Their *p*-type doping action then moves the Fermi level towards lower values. When the formation energies of interstitial and substitutional Mg become approximately equal, the concentration of Mg interstitials suddenly rises and the Fermi level is pinned through a feedback mechanism. Hence, in this scenario, the amphoteric nature of the Mg impurity is critical to explain the drop-off in the hole density observed experimentally.

Unlike the vacancy-dominated mechanism, in which variations of thermodynamic growth conditions could drastically impact the occurrence of compensation, the interstitial-dominated mechanism remains fairly insensitive to such variations leading to at most a small shift of the pinned Fermi level. However, the  $\text{Mg}_{\text{inter}}$ -driven self-compensation discussed in this work leaves open the

possibility of achieving *p*-doped GaN samples with higher hole concentrations. For this purpose, it is necessary to extrinsically control the Fermi energy during growth in such a way that the pinning of the Fermi level is reached at a higher level of Mg doping. This could for instance be achieved by increasing the electron density via UV illumination<sup>62</sup> or by electron beam irradiation. We illustrate the effect of such interventions by rigidly shifting the evolution of the Fermi energy as shown in Fig. 9(a). By consequence, the compensation due to  $Mg_{inter}$  would activate at higher Mg doping density and the hole density at room temperature could grow to higher values before reaching the drop-off [Fig. 9(d)]. Such a rationale also

provides a natural framework for explaining the higher hole densities recently achieved under modified growth conditions.<sup>9,14</sup>

## ACKNOWLEDGMENTS

We acknowledge fruitful interactions with N. Grandjean. Financial support is acknowledged from the Swiss National Science Foundation (Grants Nos. 200020-152799). We used computational resources of CSCS and CSEA-EPFL.

- 
- \* giacomo.miceli@epfl.ch
- <sup>1</sup> S. Pearton, J. Zolper, R. Shul, and F. Ren, J. Appl. Phys. **86**, 1 (1999).
  - <sup>2</sup> H. Amano, M. Kito, K. Hiramatsu, and I. Akasaki, Jpn. J. Appl. Phys. **28**, L2112 (1989).
  - <sup>3</sup> S. Nakamura, T. Mukai, and M. Senoh, Appl. Phys. Lett. **64**, 1687 (1994).
  - <sup>4</sup> O. Madelung, *Semiconductors: Data Handbook* (Springer, 2004).
  - <sup>5</sup> B. Monemar, P. P. Paskov, G. Pozina, C. Hemmingsson, J. P. Bergman, T. Kawashima, H. Amano, I. Akasaki, T. Paskova, S. Figge, D. Hommel, and A. Usui, Phys. Rev. Lett. **102**, 235501 (2009).
  - <sup>6</sup> B. Monemar, P. P. Paskov, G. Pozina, C. Hemmingsson, J. P. Bergman, H. Amano, I. Akasaki, S. Figge, D. Hommel, T. Paskova, and A. Usui, Phys. Status Solidi C **7**, 1850 (2010).
  - <sup>7</sup> B. Monemar, P. P. Paskov, G. Pozina, C. Hemmingsson, J. P. Bergman, S. Khromov, V. N. Izyumskaya, V. Avrutin, X. Li, H. Morkoç, H. Amano, M. Iwaya, and I. Akasaki, J. Appl. Phys. **115**, 053507 (2014).
  - <sup>8</sup> U. Kaufmann, P. Schlotter, H. Obloh, K. Köhler, and M. Maier, Phys. Rev. B **62**, 10867 (2000).
  - <sup>9</sup> S. Brochen, J. Brault, S. Chenot, A. Dussaigne, M. Leroux, and B. Damilano, Appl. Phys. Lett. **103**, 032102 (2013).
  - <sup>10</sup> M. Malinverni, J.-M. Lamy, D. Martin, E. Feltin, J. Dor-saz, A. Castiglia, M. Rossetti, M. Duelk, C. Vélez, and N. Grandjean, Appl. Phys. Lett. **105**, 241103 (2014).
  - <sup>11</sup> J. Neugebauer and C. G. Van de Walle, Appl. Phys. Lett. **68**, 1829 (1996).
  - <sup>12</sup> S. Nakamura, T. Mukai, M. Senoh, and N. Iwasa, Jpn. J. Appl. Phys. **31**, L139 (1992).
  - <sup>13</sup> A. Castiglia, J.-F. Carlin, and N. Grandjean, Appl. Phys. Lett. **98**, 213505 (2011).
  - <sup>14</sup> G. Namkoong, E. Trybus, K. K. Lee, M. Moseley, W. A. Doolittle, and D. C. Look, Appl. Phys. Lett. **93**, 172112 (2008).
  - <sup>15</sup> U. Kaufmann, M. Kunzer, M. Maier, H. Obloh, A. Ramakrishnan, B. Santic, and P. Schlotter, Appl. Phys. Lett. **72**, 1326 (1998).
  - <sup>16</sup> P. Kozodoy, S. Keller, S. DenBaars, and U. Mishra, J. Crys. Growth **195**, 265 (1998).
  - <sup>17</sup> C. G. Van de Walle, C. Stampfl, and J. Neugebauer, J. Crys. Growth **189**, 505 (1998).
  - <sup>18</sup> P. Kozodoy, H. Xing, S. P. DenBaars, U. K. Mishra, A. Saxler, R. Perrin, S. Elhamri, and W. Mitchel, J. Appl. Phys. **87**, 1832 (2000).
  - <sup>19</sup> S. Hautakangas, J. Oila, M. Alatalo, K. Saari-nen, L. Liskay, D. Seghier, and H. P. Gislason, Phys. Rev. Lett. **90**, 137402 (2003).
  - <sup>20</sup> S. Hautakangas, K. Saarinen, L. Liskay, J. A. Freitas, and R. L. Henry, Phys. Rev. B **72**, 165303 (2005).
  - <sup>21</sup> J. L. Lyons, A. Janotti, and C. G. Van de Walle, Phys. Rev. Lett. **108**, 156403 (2012).
  - <sup>22</sup> J. Buckeridge, C. R. A. Catlow, D. O. Scanlon, T. W. Keal, P. Sherwood, M. Miskufova, A. Walsh, S. M. Woodley, and A. A. Sokol, Phys. Rev. Lett. **114**, 016405 (2015).
  - <sup>23</sup> Q. Yan, A. Janotti, M. Scheffler, and C. G. Van de Walle, Appl. Phys. Lett. **100**, 142110 (2012).
  - <sup>24</sup> G. Miceli and A. Pasquarello, Microelectron. Eng. **147**, 51 (2015).
  - <sup>25</sup> C. Freysoldt, J. Neugebauer, and C. G. Van de Walle, Phys. Rev. Lett. **102**, 016402 (2009).
  - <sup>26</sup> H.-P. Komsa, T. T. Rantala, and A. Pasquarello, Phys. Rev. B **86**, 045112 (2012).
  - <sup>27</sup> J. Neugebauer and C. G. Van de Walle, in *Mater. Res. Soc. Symp. Proc.*, Vol. 395 (Cambridge Univ Press, 1995) p. 645.
  - <sup>28</sup> O. K. Al-Mushadani and R. J. Needs, Phys. Rev. B **68**, 235205 (2003).
  - <sup>29</sup> S. K. Estreicher, M. Sanati, D. West, and F. Ruymgaart, Phys. Rev. B **70**, 125209 (2004).
  - <sup>30</sup> B. Grabowski, T. Hickel, and J. Neugebauer, Phys. Status Solidi (b) **248**, 1295 (2011).
  - <sup>31</sup> G. Miceli, M. Ceriotti, M. Bernasconi, and M. Parrinello, Phys. Rev. B **83**, 054119 (2011).
  - <sup>32</sup> D. Chandler, *Introduction to modern statistical mechanics* (Oxford University Press, 1987).
  - <sup>33</sup> J. Heyd, G. E. Scuseria, and M. Ernzerhof, J. Chem. Phys. **118**, 8207 (2003); **124**, 219906 (2006).
  - <sup>34</sup> W. Chen and A. Pasquarello, Phys. Review B **90**, 165133 (2014).
  - <sup>35</sup> P. Giannozzi, S. Baroni, N. Bonini, M. Calandra, R. Car, C. Cavazzoni, D. Ceresoli, G. L. Chiarotti, M. Cococcioni, I. Dabo, A. Dal Corso, S. de Gironcoli, S. Fabris, G. Fratesi, R. Gebauer, U. Gerstmann, C. Gougous-sis, A. Kokalj, M. Lazzeri, L. Martin-Samos, N. Marzari, F. Mauri, R. Mazzarello, S. Paolini, A. Pasquarello, L. Paulatto, C. Sbraccia, S. Scandolo, G. Sclauzero, A. P. Seitsonen, A. Smogunov, P. Umari, and R. M. Wentzcovitch, J. Phys.: Condens. Matter **21**, 395502 (2009).
  - <sup>36</sup> H.-P. Komsa, P. Broqvist, and A. Pasquarello, Phys. Rev. B **81**, 205118 (2010).
  - <sup>37</sup> P. Broqvist, A. Alkauskas, and A. Pasquarello, Phys. Rev. B **80**, 085114 (2009).
  - <sup>38</sup> J. P. Perdew, K. Burke, and M. Ernzerhof, Phys. Rev.

- Lett. **77**, 3865 (1996).
- <sup>39</sup> L. Gordon, J. Lyons, A. Janotti, and C. Van de Walle, Phys. Rev. B **89**, 085204 (2014).
  - <sup>40</sup> S. Lany and A. Zunger, Appl. Phys. Lett. **96**, 142114 (2010).
  - <sup>41</sup> Y. Y. Sun, T. A. Abtew, P. Zhang, and S. B. Zhang, Phys. Rev. B **90**, 165301 (2014).
  - <sup>42</sup> J. Neugebauer and C. G. Van de Walle, Phys. Rev. B **50**, 8067 (1994).
  - <sup>43</sup> P. Bogusławski, E. L. Briggs, and J. Bernholc, Phys. Rev. B **51**, 17255 (1995).
  - <sup>44</sup> S. Limpijumnong and C. G. Van de Walle, Phys. Rev. B **69**, 035207 (2004).
  - <sup>45</sup> M. R. Ranade, F. Tessier, A. Navrotsky, V. J. Leppert, S. H. Risbud, F. J. DiSalvo, and C. M. Balkas, J. Phys. Chem. B **104**, 4060 (2000).
  - <sup>46</sup> A. Alkauskas, P. Broqvist, and A. Pasquarello, Phys. Rev. Lett. **101**, 046405 (2008).
  - <sup>47</sup> A. Alkauskas, P. Broqvist, and A. Pasquarello, Phys. Status Solidi B **248**, 775 (2011).
  - <sup>48</sup> A. Alkauskas and A. Pasquarello, Phys. Rev. B **84**, 125206 (2011).
  - <sup>49</sup> W. Walukiewicz, J. Vac. Sci. Technol. B **5**, 1062 (1987); Phys. Rev. B **37**, 4760 (1988).
  - <sup>50</sup> D. Colleoni, G. Miceli, and A. Pasquarello, J. Phys.: Condens. Matter **26**, 492202 (2014).
  - <sup>51</sup> Z. Benzarti, I. Halidou, Z. Bougrioua, T. Boufaden, and B. El Jani, J. Cryst. Growth **310**, 3274 (2008).
  - <sup>52</sup> S. Baroni, S. De Gironcoli, A. Dal Corso, and P. Gianozzi, Rev. Mod. Phys. **73**, 515 (2001).
  - <sup>53</sup> J. S. Blakemore, *Semiconductor statistics* (Pergamon, Oxford, 1962).
  - <sup>54</sup> D. C. Look, *Electrical Characterization of GaAs Materials and Devices* (Wiley, New York, 1989).
  - <sup>55</sup> P. Rinke, M. Winkelnkemper, A. Qteish, D. Bimberg, J. Neugebauer, and M. Scheffler, Phys. Rev. B **77**, 075202 (2008).
  - <sup>56</sup> W. Chen and A. Pasquarello, J. Phys.: Condens. Matter **27**, 133202 (2015).
  - <sup>57</sup> S. Barbet, R. Aubry, M.-A. di Forte-Poisson, J.-C. Jacquet, D. Deresmes, T. Melin, and D. Theron, Appl. Phys. Lett. **93**, 212107 (2008).
  - <sup>58</sup> H. Sezen, E. Ozbay, O. Aktas, and S. Suzer, Appl. Phys. Lett. **98**, 111901 (2011).
  - <sup>59</sup> O. Ambacher, M. Brandt, R. Dimitrov, T. Metzger, M. Stutzmann, R. Fischer, A. Miehr, A. Bergmaier, and G. Dollinger, J. Vac. Sci. Technol. B **14**, 3532 (1996).
  - <sup>60</sup> O. Ambacher, F. Freudenberger, R. Dimitrov, H. Angerer, and M. Stutzmann, Jpn. J. Appl. Phys. **37**, 2416 (1998).
  - <sup>61</sup> M. Ganchenkova and R. Nieminen, Phys. Rev. Lett. **96**, 196402 (2006).
  - <sup>62</sup> Z. Bryan, M. Hoffmann, J. Tweedie, R. Kirste, G. Callsen, I. Bryan, A. Rice, M. Bobea, S. Mita, J. Xie, Z. Sitar, and R. Collazo, J. Electron. Mater. **42**, 815 (2013).